Inhibition of cytosolic phospholipase A2α impairs an early step of coronavirus replication in cell culture

Christin Müller[1], Martin Hardt[2], Dominik Schwudke[3], Benjamin W. Neuman[4], Stephan Pleschka[1], and John Ziebuhr[1*]

[1]Institute of Medical Virology, Justus Liebig University Giessen, 35392 Giessen, Germany
[2]Imaging Unit, Biomedical Research Center, Justus Liebig University Giessen, 35392 Giessen, Germany
[3]Division of Bioanalytical Chemistry, Priority Area Infection, Research Center Borstel, Leibniz Center for Medicine and Bioscience, 23845 Borstel, Germany
[4]Texas A&M University, Texarkana, TX 75503, USA

Running Title: Role of cytosolic phospholipase $A_2\alpha$ in coronavirus replication

*Correspondence to:
John Ziebuhr, Institute of Medical Virology, Justus Liebig University Giessen,
Schubertstr. 81, 35392 Giessen, Germany
Tel: +49 (0) 641 99 41200
Fax: +49 (0) 641 99 41209
E-Mail: john.ziebuhr@viro.med.uni-giessen.de

Abstract: 246 words, Importance: 150 words
Main text: 7013 words
Figures: 9; Supplemental information: 2 tables

Abstract

Coronavirus replication is associated with intracellular membrane rearrangements in infected cells, resulting in the formation of double membrane vesicles (DMV) and other membranous structures that are referred to as replicative organelles (RO). The latter provide a structural scaffold for viral replication/transcription complexes (RTC) and help to sequester RTC components from recognition by cellular factors involved in antiviral host responses. There is increasing evidence that plus-strand (+) RNA virus replication, including RO formation and virion morphogenesis, affects cellular lipid metabolism and critically depends on enzymes involved in lipid synthesis and processing. Here, we investigated the role of cytosolic phospholipase $A_2\alpha$ ($cPLA_2\alpha$) in coronavirus replication using a small-molecular-weight non-peptidic inhibitor (Py-2). Inhibition of $cPLA_2\alpha$ activity, which produces lysophospholipids (LPL) by cleaving at the *sn*-2 position of phospholipids, had profound effects on viral RNA and protein accumulation in human coronavirus 229E-infected Huh-7 cells. Transmission electron microscopy revealed that DMV formation in infected cells was significantly reduced in the presence of the inhibitor. Furthermore, we found that (i) viral RTCs colocalized with LPL-containing membranes, (ii) cellular LPL concentrations were increased in coronavirus-infected cells and (iii) this increase was diminished in the presence of $cPLA_2\alpha$ inhibitor Py-2. Py-2 also displayed antiviral activities against other viruses representing the *Coronaviridae* and *Togaviridae* families, while members of the *Picornaviridae* were not affected. Taken together, the study provides evidence that $cPLA_2\alpha$ activity is critically involved in the replication of various +RNA virus families and may thus represent a candidate target for broad-spectrum antiviral drug development.

53 **Importance**

54

55 Examples of highly conserved RNA virus proteins that qualify as drug targets for broad-
56 spectrum antivirals remain scarce, resulting in increased efforts to identify and specifically
57 inhibit cellular functions that are essential for the replication of RNA viruses belonging to
58 different genera and families. The present study supports and extends previous conclusions
59 that enzymes involved in cellular lipid metabolism may be tractable targets for broad-
60 spectrum antivirals. We obtained evidence to show that a cellular phospholipase, cPLA2α,
61 which releases fatty acid from the *sn*-2 position of membrane-associated
62 glycerophospholipids, is critically involved in coronavirus replication, most likely by producing
63 lysophospholipids that are required to form the specialized membrane compartments at
64 which viral RNA synthesis takes place. The importance of this enzyme in coronavirus
65 replication and DMV formation is supported by several lines of evidence, including confocal
66 and electron microscopy, viral replication and lipidomics studies of coronavirus-infected cells
67 treated with a highly specific $cPLA_2\alpha$ inhibitor.

68

69 **Introduction**

70 *Coronavirinae* are a subfamily of enveloped, positive-sense (+) RNA viruses in the family
71 *Coronaviridae* that, together with the *Arteri*-, *Roni*-, and *Mesoniviridae*, belongs to the order
72 *Nidovirales* (1, 2). Coronavirus infections in humans are mainly associated with (common
73 cold-like) upper respiratory tract infections and are caused by 4 coronavirus species that
74 have been classified as members of the genera *Alphacoronavirus* (Human coronavirus 229E
75 [HCoV-229E], Human coronavirus NL63 [HCoV-NL63]) and *Betacoronavirus* (Human
76 coronavirus OC43 [HCoV-OC43], Human coronavirus HKU1 [HCoV-HKU1]) (1, 3). In
77 contrast to these common human coronaviruses, infections with zoonotic coronaviruses,
78 such as severe acute respiratory syndrome (SARS) coronavirus (SARS-CoV) (4, 5) and
79 Middle East respiratory syndrome (MERS) coronavirus (MERS-CoV) (6), may lead to much
80 more severe or even fatal respiratory disease in humans as illustrated by the SARS outbreak
81 in 2002/2003 (5, 7) and, more recently, a significant number of cases with acute respiratory
82 distress syndrome caused by MERS-CoV, which have been recorded over the past 5 years
83 (8).
84
85 Similar to other +RNA viruses, coronavirus replication involves extensive membrane
86 rearrangements in infected cells, resulting in the formation of large, organelle-like “virus
87 factories” to which the multi-subunit viral replication/transcription complexes (RTCs) are
88 anchored (reviewed in (9, 10)). These replicative organelles (ROs) are thought to provide a
89 structural scaffold for the viral RNA synthesis machinery and contribute to sequestering
90 components of this machinery from host defense mechanisms, suggesting important roles for
91 ROs in viral replication (9, 11-13). RO formation in coronavirus-infected cells requires three
92 replicase gene-encoded nonstructural proteins (nsp), called nsp3, nsp4, and nsp6, that all
93 contain conserved transmembrane domains (14-17). Electron microscopy/tomography
94 studies revealed that coronavirus-induced membrane rearrangements result in multiple
95 paired-membrane structures, including double membrane vesicles (DMVs) and convoluted
96 membranes that appear to be connected to the rough endoplasmic reticulum (ER) (18-24).

These ROs show remarkable parallels among different +RNA viruses that, for example, belong to the *Flaviviridae, Picornaviridae,* and *Togaviridae* families and perhaps also DNA viruses that replicate in the cytoplasm, such as *Poxviridae* (11, 25). The molecular mechanisms and factors involved in the formation of these membranous structures are poorly understood and the roles of specific membrane structures, lipid and protein components, and enzymes involved in their production remain to be studied in more detail. Consistent with the ER being the most likely membrane donor for coronaviral DMVs, cellular factors associated with ER-to-Golgi trafficking and early secretory pathways (e.g., PDI, Sec61a, EDEM1, OS-9) have been reported to be involved in SARS-CoV and mouse hepatitis virus (MHV)-induced RTC formation (22, 26, 27). Also, a potential role of autophagy in coronaviral DMV formation has been discussed, even though a number of conflicting data make it difficult to draw definitive conclusions at this stage (28). At least partly, the observed differences may be related to different cell lines and viruses used in these studies (29).

Given the major membrane rearrangements occurring in virus-infected cells, enzymes involved in cellular lipid metabolism have been suggested to play a major role in this process. In line with this, fatty acid synthase (FASN), which is a key enzyme in the fatty acid biosynthetic pathway, was shown to be recruited to Dengue virus (DENV) replication complexes (30). Moreover, pharmacological inhibition of FASN by trans-4-carboxy-5-octyl-3-methylenebutyrolactone (C75) or cerulenin resulted in impaired DENV, hepatitis C virus (HCV), West Nile virus (WNV), yellow fever virus (YFV), and vaccinia virus (VV) replication (30-35).

In this work, we extend these studies by reporting an essential role for cytosolic phospholipase $A_2\alpha$ ($cPLA_2\alpha$) in the production of DMV-associated coronaviral RTCs. This enzyme belongs to the phospholipase A_2 (PLA_2) superfamily of lipolytic enzymes, which (among several other families) includes the secretory PLA_2s ($sPLA_2$), Ca^{2+}-independent PLA_2s ($iPLA_2$), and Ca^{2+}-dependent cytosolic PLA_2s ($cPLA_2$), with the latter including $cPLA_2\alpha$

(36, 37). PLA_2s catalyze the hydrolysis of glycerophospholipids at the *sn*-2 ester bond, generating a free fatty acid and a lysophospholipid (LPL) (37, 38). $cPLA_2\alpha$ has a molecular mass of 85 kDa and preferentially hydrolyzes phospholipids that carry arachidonic acid (AA) at the *sn*-2 position. The activity of $cPLA_2\alpha$ and its translocation to intracellular membranes is regulated by Ca^{2+} binding and phosphorylation at Ser-505 by mitogen-activated protein (MAP) kinase (39). In a previous study, $cPLA_2\alpha$ activity was shown to be critically involved in the production of infectious progeny of HCV and DENV, while the activity was dispensable for vesicular stomatitis virus (VSV), a member of the *Rhabdoviridae*, suggesting distinct requirements for this lipolytic enzyme in the replication and assembly of different families of RNA viruses (40).

In this study, we report that the specific inhibition of $cPLA_2\alpha$ activity has detrimental effects on coronavirus replication. In the presence of pyrrolidine-2 (Py-2, compound 4d, (41)), a highly specific inhibitor of $cPLA_2\alpha$, the formation of DMVs and DMV-associated RTCs was significantly reduced in HCoV-229E-infected Huh-7 cells. Also, viral protein and RNA accumulation and production of infectious virus progeny was drastically diminished in the presence of non-cytotoxic concentrations of Py-2. Moreover, viral RTCs were shown to colocalize with LPL-containing membrane structures using confocal microscopy. Lipidomics studies revealed that LPL concentrations are increased in coronavirus-infected cells and that this phenotype is suppressed by Py-2. Taken together, our data suggest that LPLs produced by $cPLA_2\alpha$ may be involved in DMV formation. The study also shows that $cPLA_2\alpha$ activity is required for efficient replication of MERS-CoV and Semliki forest virus (SFV), while poliovirus (PV), human rhinovirus 1A (HRV1A), VV, and influenza A virus (IAV) replication was not affected in the presence of the cPLA2α inhibitor. In summary, our data lead us to conclude that $cPLA_2\alpha$ is an important cellular factor acting at specific steps of the replication cycle of viruses from different +RNA virus families.

153 **Material and Methods**

154 **Cells and viruses**

155 Human hepatoma cells (Huh-7), human lung fibroblasts (MRC-5), African green monkey
156 kidney cells (Vero and CV-1), baby hamster kidney cells (BHK-21), human lung epithelial
157 cells (A549), human bronchial epithelial cells (BEAS-B2), human cervix epithelial cells
158 (HeLa) and Madin Darby canine kidney cells (MDCK-II) were grown in Dulbecco's modified
159 Eagle's medium (DMEM) supplemented with 10% fetal bovine serum (FBS), 100 U/ml
160 penicillin and 100 µg/ml streptomycin at 37 °C and in an atmosphere containing 5% CO_2.
161 HCoV-229E, HRV1A, influenza virus A/Giessen/06/09 (H1N1), SFV, PV type 1 (strain
162 Mahoney) and VV (strain WR) were obtained from the virus collection of the Institute of
163 Medical Virology, Giessen, Germany. MERS-CoV (EMC/2012) was kindly provided by
164 Christian Drosten, Bonn, Germany.

165

166 **Drugs and assays**

167 The cell-permeable pyrrolidine derivative Py-2 ($C_{49}H_{44}F_2N_4O_5S$, 840 g/mol; cat. no. 525143),
168 a highly specific cPLA$_2\alpha$ inhibitor, was purchased from Merck Millipore (compound 4d; (41).
169 Arachidonyltrifluoromethane (AACOCF3, $C_{21}H_{31}F_3O$, 356.5 g/mol), an analog of AA that
170 inhibits cPLA$_2$ by direct binding (42), was obtained from Santa Cruz Biotechnology. The MEK
171 inhibitor U0126 and the p38 MAPK inhibitor SB202190 were purchased from Selleckchem.
172 The lipoxygenase inhibitor 2-(1-Thienyl)ethyl 3,4-dihydroxybenzylidenecyanoacetate (TEDC-2)
173 was purchased from Tocris Bioscience. Compounds were stored at 4 °C as 2 mM (Py-2), 10
174 mM (AACOCF3), 20 mM (SB202190) and 50 mM (U0126, TEDC-2) stock solutions,
175 respectively, in dimethyl sulfoxide (DMSO).

176

177 Cell viability in the presence of specific drugs was determined in a 96-well format by MTT
178 assay (43). Briefly, nearly confluent cell monolayers were incubated with cell culture medium
179 containing the respective drug at the indicated concentration. At the indicated time points, the
180 culture medium was replaced with 200 µl MTT mix (DMEM containing 10% FBS and 175

µg/ml tetrazolium bromide, Sigma). Following incubation for 90 min at 37 °C, the cells were fixed with 3.7% paraformaldehyde (PFA, Roth) in PBS for 30 min. Then, the fixing solution was removed and 200 µl isopropanol was added to each well. Formazan formation was measured by determining the absorbance at 490 nm using a spectrophotometer (BioTek).

To determine antiviral effects of drugs, confluent cell monolayers of Huh-7 (for HCoV-229E, MERS-CoV, VV), MRC-5 and BEAS-B2 (for HCoV-229E), HeLa (for HRV1A), BHK-21 (for SFV), A549 (for IAV H1N1) and Vero (for PV, MERS-CoV) cells, respectively, were infected at a multiplicity of infection (MOI) of 3. After 2 h, the virus inoculum was removed, cells were rinsed with phosphate-buffered saline (PBS) and fresh medium containing the indicated concentrations of Py-2 and AACOCF3, respectively, or DMSO (solvent control) was added. At 12 h p.i., the cell culture supernatant was collected. Antiviral activities of SB202190, TEDC-2 and U0126 were determined using identical conditions except that cell culture supernatants were collected at 24 h p.i. in this case. After short-term storage at -80 °C, the cell culture supernatants were used for virus titration.

Virus titration

Focus-forming assays were used to determine titers of IAV and coronaviruses**.** Briefly, Huh-7 (for CoVs) or MDCK (for IAV H1N1) cells were seeded in 96-well plates. At 90% confluency, the medium was removed, the cells were washed with PBS++ (PBS containing 1 mM $MgCl_2$, 0.9 mM $CaCl_2$) and inoculated for 1 h at 33 °C with 10-fold serial dilutions of virus-containing cell culture supernatants in PBS++/BA/P/S (PBS containing 0.2% bovine serum albumin [BSA], 1 mM $MgCl_2$, 0.9 mM $CaCl_2$, 100 U/ml penicillin and 100 mg/ml streptomycin). Next, the virus inoculum was replaced with Minimum Essential Medium (MEM) containing 1.25% Avicel (FMC Biopolymer) for 24-48 h. For IAV, 1 µg/ml trypsin was included in this medium. Next, the Avicel-containing medium was removed, cells were washed with PBS and then fixed and permeabilized for 30 min with PBS containing 3.7% PFA and 1% Triton X-100. The cells were washed again with PBS and incubated with 50 µl of the appropriate primary

antibody solution: anti-HCoV-229E-N mouse monoclonal antibody (mAb) (M.30.HCo.I1E7, INGENASA, 1:5000 dilution), rabbit anti-MERS-CoV-N polyclonal antiserum (100211-RP02-50, Sinobiological Inc., 1:200) and mouse anti-IAV-NP mAb (1:6000, kindly provided by S. Ludwig, Münster), respectively, each diluted in PBS containing 0.1% Tween 20 (PBST). Following incubation for 1 h at room temperature, the cells were washed 3 times and incubated with the appropriate secondary antibody (goat anti-mouse IgG-HRP [sc-2005] or goat anti-rabbit IgG-HRP [sc-2004], Santa Cruz Biotechnology, 1:1000 in PBST) for 1 h at room temperature. The cells were washed again with PBS, stained with AEC staining kit (Sigma), air dried, and focus numbers were determined.

To determine virus titers by plaque assay, Huh-7 (for HCoV-229E, MERS-CoV), HeLa (for HRV1A), Vero (for PV), CV-1 (for VV) and BHK-21 (for SFV) cells, respectively, were seeded in 6-well plates and inoculated with 10-fold serial virus dilutions in PBS++/BA/P/S for 1 h. Next, the virus inoculum was replaced with Avicel-containing medium (see above). At 2-4 d p.i., the medium was removed and cells were washed with PBS and fixed with 3.7% PFA in PBS. The cell monolayer was stained with 0.15% crystal violet in PBS and plaques were counted.

Western blot analysis

Huh-7 cells were infected with HCoV-229E at an MOI of 3 and incubated in medium containing the indicated concentrations of $cPLA_2\alpha$ inhibitor or DMSO (solvent control). At 12 h p.i., the cells were lysed in Triton lysis buffer (TLB: 20 mM Tris-HCl, pH 7.4, 137 mM NaCl, 10% glycerol, 1% Triton X-100, 2 mM EDTA, 50 mM sodium glycerophosphate, 20 mM sodium pyrophosphate, 5 µg/ml aprotinin, 5 µg/ml leupeptin, 1 mM sodium vanadate, 5 mM benzamidine). Proteins were separated by SDS-polyacrylamide gel electrophoresis (PAGE) in a 10% gel and transferred onto a 0.45 µm pore-size nitrocellulose membrane (Protran, Amersham). Membranes were incubated for 1 h at room temperature with appropriate primary antibodies diluted in PBS containing 3% BSA: mouse anti-HCoV-229E-N-specific

mAb (1:1000, M.30.HCo.I1E7, INGENASA); HCoV-229E nsp8-specific rabbit serum (1:1000) (44), mouse anti-β-actin mAb (1:10.000, ab8226, Abcam) and rabbit anti-β-actin polyclonal antibody (1:10.000, ab8227, Abcam). After extensive washing with PBS, the membrane was incubated with goat anti-rabbit IRDye 800CW (1:10.000, 926-32211, LI-COR) and goat anti-mouse IRDye 680CW (1:10.000, 926-68070, LI-COR) polyclonal antibodies for 1 h at room temperature. After another wash step, the membranes were dried and the immunostained proteins were analyzed and quantified using a LI-COR Odyssey imaging system and software.

Northern blot analysis of intracellular viral RNA

Total cellular RNA from infected cells was isolated by using TRIzol reagent (ThermoFisher Scientific) according to the manufacturer's instructions, and Northern hybridization was done as described previously (45) using a [^{32}P]-labeled DNA probe specific for HCoV-229E nucleotides 26857-27235.

Immunofluorescence analysis of viral RTCs

Huh-7 cells were infected with HCoV-229E at an MOI of 3 and incubated in medium containing 20 µM Py-2 or DMSO (solvent control). At, 12 p.i., the cells were fixed and stained with mouse anti-dsRNA mAb (1:100, J2, SCICONS English & Scientific Consulting Kft.), mouse anti-HCoV-229E-N mAb (1:100, M.30.HCo.I1E7, INGENASA) and rabbit anti-HCoV-229E-nsp8 polyclonal antiserum (1:100) (44). As secondary antibodies, Alexa Fluor 594 goat anti-mouse IgG (H+L) and Alexa Fluor 488 F(ab')2-goat anti-rabbit IgG (H+L) (1:500; A11005, A11070, Invitrogen) were used. Antibodies were diluted in PBS containing 3% BSA. For colocalization studies of viral RTCs with lysophospholipids produced by cellular PLA_2 activities, Huh-7 cells were treated with the fluorogenic PLA_2 substrate, Red/Green BODIPY phospholipid PC-A2 (A10072, Invitrogen), according to the manufacturer's instructions. Briefly, 30 µl of 10 mM DOPC (Avanti Polar Lipids), 30 µl of 10 mM DOPG (Avanti Polar Lipids), and 30 µl of 1 mM PC-A2 (each prepared using ethanol as solvent) were mixed. 77

265 µl of this ethanolic lipid mix was injected under rapid stirring into 5 ml of buffer containing 50
266 mM Tris-HCl, 100 mM NaCl, 1 mM $CaCl_2$ (pH adjusted to 8.9). Next, this liposomally
267 incorporated substrate mix was added to the cells for 15 min at 10°C. Thereafter, the cells
268 were infected with HCoV-229E with an MOI of 3. At 12 h p.i., the cells were fixed and stained
269 using a dsRNA-specific mAb (see above). Colocalization studies of dsRNA with newly
270 synthesized RNA were done according to Hagemeijer et al. (20). Briefly, Huh-7 cells grown
271 on glass coverslips were infected with HCoV-229E at an MOI of 3. At 2 h p.i., the virus
272 inoculum was replaced with medium containing 20 µM Actinomycin D (Sigma) to block
273 cellular DNA-dependent RNA synthesis. At 11 h p.i., 1 mM 5-ethynyl uridine (5-EU;
274 Invitrogen) was included in the medium. At 12 h p.i, the cells were fixed with 3.7 % PFA in
275 PBS and permeabilized using 0.1 % Triton X-100. Incorporation of the alkyne-modified
276 uridine analog, 5-EU, was visualized using click chemistry according to the manufacturer's
277 instructions (Click-iT RNA Alexa Fluor 594 Imaging Kit, Invitrogen). In addition, the cells were
278 stained using a dsRNA-specific antibody as described above.

279 Images were acquired by confocal laser-scanning microscopy (Leica TCS SP5, Leica). For
280 colocalization analysis, hardware prerequisites and settings were carefully observed. For
281 imaging, a 63x Plan-Apochromate objective (λ corrected; NA = 1.4) was used and the
282 pinhole aperture was set to 1 airy unit (AU = 1), resulting in an optical section thickness of
283 0.772 µm. Intensities of laser lines used for excitation were kept rather low to minimize
284 possible bleaching effects. Gain and offset of the PMTs were optimized for each channel
285 using lookup table (LUT) functions in order to adapt thresholds and to prevent clipping of
286 high-intensity signals. The frames of the different channels were recorded sequentially and
287 care was taken to ensure clear spectral separation of the signals analyzed and to exclude
288 any crosstalk and bleedthrough between channels.

289 Data were processed using the Imaris 8.4 software package (Bitplane). Colocalization
290 analysis of dsRNA signals with signals of PC-A2 and $cPLA_2\alpha$-mediated cleavage
291 products was based on correlating intensities in the different channels according to

Pearson's colocalization coefficient (PCC), taking advantage of PCC being highly independent from background levels and signal brightness (46). Values of 1, -1, and 0 indicate perfect colocalization, strict exclusion and random localization, respectively, as described previously (47-50). Colocalization volumes and rates were calculated for total images using automated threshold settings (51).

Electron microcopy

Huh-7 cells were grown on ACLAR film (Agar Scientific). Following infection with HCoV-229E at an MOI of 3 (or mock infection) for 2 hours, the cell culture medium was replaced with fresh medium containing 20 µM Py-2 (or the appropriate amount of DMSO as a control). After 12 h, at 33 °C, the cell culture medium was removed. The cells were washed with PBS and fixed with 3% formaldehyde and 1% glutaraldehyde in 0.1M PBS and post fixed in 1% osmium tetroxide. After incubation in 1% aqueous uranyl acetate (Polysciences), specimens were dehydrated in an ethanol series (30, 50, 70, 80, 90, 96, 100% [v/v], 20 min each) and embedded in Epon (Serva). From the blocks cured by heat silver-to-gold ultrathin sections were cut and subsequently contrasted in uranyl acetate and lead citrate. Ultrathin sections were inspected in the TEM (EM912a/b - ZEISS) at 120kV under zero-loss conditions and images were recorded at slight underfocus using a cooled 2k x 2k slow-scan ccd camera (SharpEye / TRS) and the iTEM package (Olympus-SIS). All experiments were done in biological duplicates. For statistical analysis, at total of >100 ultrathin sections from different cells were analyzed in each experiment.

Lipidome analysis

Huh-7 cells were mock infected or infected with HCoV-229E at an MOI of 3 and incubated in medium containing (or lacking) Py-2 (20 µM, 2-12 h p.i.). As additional controls, (i) untreated/mock-infected cells and (ii) cells inoculated with UV-inactivated HCoV-229E were used. UV-inactivated virus was obtained by exposing an aliquot of the same virus stock to UV light (Philips, TUV 15W/G15 T8) for 3 h. Inactivation of virus infectivity was confirmed by

plaque assay. At 12 h p.i., cells were collected and subjected to cellular lipidome analysis. Briefly, lipids were extracted using methyl-*tert*-butyl ether as described earlier (52) and analyzed using a Q-Exactive Plus (Thermo Scientific) using the shotgun lipidomics approach and LipidXplorer (53-56). Lipids were quantified using an internal standard mix (Supplemental Table 2) following the lipidomics screen approach. Lipid abundances were calculated using the respective standards and normalized to cell number (Supplemental Tables 1 and 2). Experiments were performed using 8 biologically independent replicates for each group except for the group of HCoV-229E-infected, untreated cells (7 replicates). Statistics analyses were done using the two-tailed unpaired Student's *t* test.

Results

cPLA$_2\alpha$ activity is required for HCoV-229E replication

cPLA$_2\alpha$ inhibition by Py-2 (20 µM) was previously reported to reduce the production of infectious virus progeny of different members of the *Flaviviridae*, as shown for HCV and DENV (40). We now investigated if Py-2 also affects the replication of other +RNA viruses, such as coronaviruses (using HCoV-229E and MERS-CoV). First, we sought to confirm that Py-2 has no cytotoxic effects in Huh-7, MRC-5 and BEAS-B2 cells at concentrations shown previously to have strong antiviral affects (40). We found that cell viability was not affected by Py-2 concentrations of up to 40 µM (Fig. 1A). Next, we determined the effect of Py-2 on HCoV-229E reproduction. As shown in Fig. 1B, treatment with Py-2 resulted in reduced viral titers in a dose-dependent manner, with nearly 100-fold reduction of HCoV-229E titers produced from Huh-7 cells treated with 20 µM Py-2. HCoV-229E replication in the presence of 20 µM Py-2 was also found to be reduced using MRC-5 (Fig.1C) and BEAS-B2 (Fig.1D) cells, suggesting that the observed antiviral effect of Py-2 is not cell type specific. As shown in Fig. 1E, the reduced production of infectious virus progeny at 12 h p.i. could also be confirmed for later time points (15, 21, 24 h) p.i., suggesting a profound inhibition (rather than delay) of viral replication by this cPLA$_2$ inhibitor.

In line with the Py-2 inhibition data, a second cPLA$_2$ inhibitor, AACOCF3, was confirmed to reduce HCoV-229E replication at non-toxic concentrations (Fig. 2A, B). Most likely, the slightly lower efficacy of AACOCF3 resulted from its lower specificity as discussed earlier (40). Similar antiviral effects on HCoV-229E replication were also observed for inhibitors of p38 MAP kinase and MEK, two important activators of cPLA$_2\alpha$ (Fig. 2C), but not for inhibitors of enzymes acting downstream of cPLA$_2\alpha$ in arachidonic acid (AA)-dependent pathways, such as cyclooxygenases 1/2 (COX 1/2) and lipoxygenase (LOX) (Fig. 2D;(57)), that metabolize AA to produce important inflammation mediators. Taken together, the data

support a critical role of (activated) cPLA$_2\alpha$ in HCoV-229E replication, suggesting that this lipolytic enzyme has a more general role in +RNA virus replication than previously thought.

To identify critical steps of the coronavirus life cycle that are affected by cPLA2α inhibitors, we characterized viral protein accumulation in infected cells by Western blotting and immunofluorescence analysis. As shown in Fig. 3 (A, B), accumulation of HCoV-229E structural (N) and nonstructural (nsp8) proteins was reduced in the presence of the drug, with nearly no viral proteins being detectable at 20 µM Py-2. In line with this, we found a significantly reduced accumulation of viral RNAs in infected cells treated with the cPLA$_2\alpha$ inhibitor (Fig. 3C). These data suggest that, unlike the situation in HCV and DENV (40), cPLA$_2\alpha$ activity may be required for an early step in coronavirus replication. To investigate if viral entry or other early steps in viral replication are affected by the drug, we performed a time-of-addition experiment (Fig. 3D). For this purpose, Py-2 (20 µM) was included in the cell culture medium during virus adsorption (until 2 h p.i.) or at later time points p.i. (between 2-6, 4-8, 6-10, and 8-12 h p.i., respectively). To determine the total infectious virus progeny produced until 12 h p.i. (with Py-2 being added at different time points), cell culture supernatants collected over time for a given experiment were pooled and virus titers were determined by focus-forming assay. The presence of Py-2 in the culture medium between 0 and 2 h p.i. had no effect on virus titers, indicating that cPLA$_2\alpha$ activity is not required for viral entry. In contrast, the presence of Py-2 between 2-6 h p.i. caused a massive reduction of virus titers, while less profound effects were observed if the drug was present in the culture medium later in infection (Fig. 3D). The observed time-dependent effects of Py-2 on the production of infectious HCoV-229E progeny lead us to suggest that cPLA$_2\alpha$ activity is important for an early step of coronavirus replication but not for entry itself.

cPLA$_2\alpha$ inhibition prevents the formation of viral RTCs

As described above, a profound antiviral effect was observed for Py-2 when given between 2 and 6 h p.i., suggesting that the formation of RTCs and their integration into rearranged

386 cellular membranes may be affected by the drug. We therefore investigated potential effects
387 of Py-2 on the formation of ROs in HCoV-229E-infected cells. Coronavirus RTCs are known
388 to produce a typical perinuclear staining pattern when analyzed by immunofluorescence
389 microscopy using reagents that detect double-stranded (ds) RNA and viral replicative
390 proteins. In the presence of 20 μM Py-2, the typical punctate perinuclear staining described
391 previously for HCoV-229E RTC components in virus-infected cells (44, 58) was greatly
392 diminished (Fig. 4). The profound reduction in both size and numbers of viral ROs was even
393 more evident in 3D reconstructions of Z-stacks obtained from infected/untreated and
394 infected/treated cells, respectively (Fig. 5A).
395
396 Although dsRNA and replicase gene-encoded nsps are accepted to be key components of
397 viral RTCs and, therefore, have been widely used as markers to localize intracellular sites of
398 viral RNA synthesis, a number of betacoronavirus studies showed that (i) dsRNA, (ii) newly
399 synthesized RNA, (iii) RTC components and (iv) (some) virus-induced membrane
400 compartments may not always colocalize perfectly, particularly, at later time points p.i. (20,
401 24). We therefore decided to perform an additional experiment to answer the question of
402 whether dsRNA and nascent RNA are equally suitable for detecting intracellular sites of RNA
403 synthesis at 12 h p.i., that is, the time point used in the present study for HCoV-229E-
404 infected Huh-7 cells. To this end, we conducted an immunofluorescence study of nascent
405 RNA synthesis by click chemistry using the uridine analog 5-EU (59) and (co-)stained the
406 sites of dsRNA accumulation using a dsRNA-specific antibody. As shown in Fig. 5B, we were
407 able to show that dsRNA and nascent RNA colocalize very well, suggesting that (most)
408 dsRNA-containing structures represent ROs actively engaged in viral RNA synthesis, at
409 least, at this particular time point. Taken together, our data lead us to suggest that the
410 formation of DMV-associated RTCs in HCoV-229E-infected cells is reduced in Py-2-treated
411 cells.
412

To further corroborate this hypothesis, we studied DMV formation by transmission electron microscopy (Fig. 6). Intracellular virions (ICVs) were detected in approximately 50% of the cells analyzed per section and DMVs were found in approximately 40% of the cells analyzed per section in HCoV-229E-infected Huh-7 cells at 12 h p.i. (Fig. 6A, B, and E). In contrast, significantly less DMVs were detected if the virus-infected cells were treated with Py-2 (Fig. 6C and D), with only 20% of the cells containing DMVs and 10-15% containing ICVs (Fig. 6E). In infected/untreated cells, we regularly observed DMV clusters of around 15 DMVs. As a result of Py-2 treatment, the number of DMVs per cell section dropped significantly to about 5 DMVs per cell (Fig. 6F). This phenotype was most evident in cells treated with Py-2 early in infection, starting at 2 p.i.. There was no major difference observable between cells treated with Py-2 for 5 and 10 hours, respectively (compare 2-7 and 2-12 p.i.; Fig. 6E and F). In both cases, the numbers of DMVs and ICVs per cell were significantly reduced**.** In contrast, if cPLA$_2\alpha$ activity was inhibited at later time points p.i. (between 7 and 12 h p.i.), DMV formation was not significantly affected compared to untreated HCoV-229E-infected cells. The data suggest an important role for cPLA$_2\alpha$ activity in the process of DMV formation occurring early in infection, while this activity appears to be less critical if sufficient numbers of DMVs have already been formed (Fig. 6E and F).

Colocalization of coronavirus RTCs with LPLs

cPLA$_2\alpha$ cleaves glycerophospholipids at the *sn*-2 position, generating an LPL and releasing AA. The latter is a key inflammatory intermediate and important precursor that is metabolized by multiple enzymes including cyclooxygenases (COX) 1/2 and 5-lipoxygenase (LOX), leading to the production of prostaglandines, thromboxanes, leukotrienes and many other inflammation mediators. As shown in Fig. 2D and a previous study (57), we failed to obtain evidence for anti-coronaviral activities of LOX and COX 1/2 inhibitors, arguing against a major role of AA (and its downstream metabolites) in coronavirus replication. We therefore considered it more likely that the other product of PLA$_2\alpha$ activity (i.e., the LPL) has a role in supporting viral replication, for example, by providing specific lipid components required to

441 form viral ROs. To address the latter possibility, we made use of a fluorogenic
442 phosphatidylcholine (PC-A2) with (quenched) fluorophores attached to each of the two fatty
443 acids. Following liposome-mediated uptake of PC-A2 and cPLA$_2\alpha$-mediated cleavage of the
444 fatty acid attached to the *sn*-2 position of this fluorogenic substrate, the subcellular
445 localization of the resulting LPL was monitored by confocal laser-scanning microscopy. To
446 investigate a possible colocalization of LPLs and viral RTCs, PC-A2-treated and infected
447 cells were fixed and a dsRNA-specific antibody was used as a marker for RTCs. As shown in
448 Fig. 7**,** viral RTCs were detected with their typical perinuclear staining pattern (see also Fig.
449 4). A careful inspection revealed that, although the LPL and dsRNA clusters, respectively,
450 vary with respect to size and spatial distribution, there was a high degree of colocalization of
451 dsRNA with LPL signals (but not vice versa), which is also supported by our calculations of
452 PCCs and colocalization rates. This colocalization of RTCs with LPLs is also illustrated by
453 the signals displayed in the extra 'colocalization channel' shown to the right (Fig. 7, right
454 column), with colocalization signals strongly resembling the signals obtained for the dsRNA
455 clusters alone. The high colocalization rates and PCC values revealed by our analysis
456 strongly support the hypothesis that LPLs produced by cPLA$_2\alpha$ are integral parts of DMVs. It
457 should also be noted that the colocalization rates indicated in Fig. 7 are based on an
458 automated and rather cautious method of calculation (see Materials and Methods). LPL
459 signals that do not colocalize with dsRNA presumably originate from other intracellular
460 membrane structures, such as endocytotic vesicles.
461
462 **Lipidome analysis of infected cells**
463 To gain more insight into the roles of lipids in coronavirus replication and DMV formation, we
464 performed comparative lipidome analyses of (i) Huh-7 cells, (ii) Huh-7 cells incubated with
465 UV-inactivated HCoV-229E, (iii) Huh-7 cells infected with HCoV-229E and (iv) Huh-7 cells
466 infected with HCoV-229E and treated with Py-2, and (v) Huh-7 cells treated with Py-2 (Fig.
467 8). Lipids were isolated at 12 h p.i., at a time when, under optimal conditions, DMVs have
468 been formed (Figs. 4, 5, and 6) and large amounts of viral genomic and subgenomic RNAs

469 have been produced (Fig. 3C). We monitored the abundances of 359 lipids of 14 classes
470 covering membrane lipid classes and neutral lipids (Supplemental Tables 1 and 2).
471
472 The study provided evidence that a number of changes in the cellular lipidome occur in
473 HCoV-229E-infected cells when compared to both the mock control and cells incubated with
474 UV-inactivated HCoV-229E. Our data revealed no significant change in the total abundance
475 of membrane lipids (Fig. 8A) and neutral lipids (triacylglycerols, diacylglycerols, and
476 cholesterylesters) (Fig. 8B). We however observed that Py-2 treatment reduced the
477 abundance of membrane lipids by approximately 25 percent, when compared to (untreated)
478 HCoV-229E-infected or mock-infected cells (Fig. 8A). Further analyses of the lipid profiles
479 revealed that the phosphatidic acid (PA) abundance was decreased in Py-2-treated and in
480 HCoV-229E-infected Huh-7 cells at 12 h p.i. (Fig. 8C). For ceramides (Cer), an increased
481 abundance was detected in Py-2-treated and in HCoV-229E-infected cells (Fig. 8D).
482 However, Py-2 treatment of infected cells did not alter the ceramide content any further,
483 suggesting that Cer- and PA-associated metabolic pathways in HCoV-229E-infected cells
484 are not (or only marginally) affected by the cPLA$_2\alpha$ activity.
485
486 For many lysophospholipid species (LPL), most prominently lysophosphatidylethanolamine
487 (LPE) and lysophosphatidylinositols (LPI), a correlation between Py-2 treatment and
488 inhibition of viral replication and lipid quantities was observed (Fig. 8E, Supplemental Table
489 1). The total cellular LPL content was found to be reduced upon treatment with Py-2,
490 supporting a specific role of cPLA$_2\alpha$ in generating these LPLs. For HCoV-229E infected cells,
491 the LPL content was increased in comparison to cells incubated with UV-treated HCoV-
492 229E, indicating that increased LPL production occurs after viral entry and requires a
493 replication-competent virus. Additionally, inhibition of cPLA$_2\alpha$ activity in HCoV-229E-infected
494 cells suppressed the replication-associated increase of LPLs, resulting in an LPL content that
495 was similar to that (i) of cells inoculated with UV-treated HCoV-229E and (ii) the mock
496 control. Finally, we found a correlation between the cellular phosphatidylglycerol (PG)

content and viral replication (Fig. 8F). The level of PG was 2-fold increased in HCoV-229E-infected cells while Py-2 treatment during viral infection resulted in a PG level similar to the control (UV-inactivated virus). Py-2 treatment alone had a minor effect on (total) PG abundances. However, PG species with shorter acyl chain lengths, such as PG 30:1 / PG 32:2 / PG 32:1 and PG 32:0, were clearly affected by the inhibitor and also showed significantly increased levels in cells incubated with UV-treated HCoV-229E (Supplemental Table 1), indicating cellular responses in lipid metabolism to viral receptor binding and/or entry that, at least in part, might overlap with redirections of specific metabolic networks caused by the inhibition of $PLA_2\alpha$ activity.

Taken together, these results show that coronavirus replication stimulates cellular LPL production which, together with the $PLA_2\alpha$ inhibition data presented above, supports the idea that LPLs play an important role in DMV formation and viral replication.

Effect of $cPLA_2\alpha$ inhibition on the replication of other viruses. The observed critical role of $cPLA_2\alpha$ activity in modulating cellular membrane structures and total LPL content in HCoV-229E-infected cells prompted us to investigate potential antiviral effects of $cPLA_2\alpha$ inhibitors on other viruses, including viruses that are known to rearrange intracellular membrane structures and compartments. First, we analyzed the effect of Py-2 treatment on another coronavirus, MERS-CoV, which, due to its pathogenicity and the large number of MERS-related deaths, has attracted significant attention (8). For MERS-CoV, a drastic inhibition of viral replication in Huh-7 and Vero cells was observed in the presence of Py-2, demonstrating that $cPLA_2\alpha$ has an equally important role for alpha- and betacoronavirus replication (Fig. 9A). An antiviral effect of Py-2 could also be confirmed for SFV (Fig. 9B), suggesting that $cPLA_2\alpha$ activity may also be involved in the replication of members of the family *Togaviridae.* In contrast, virus reproduction of other viruses included in this study was not affected by Py-2. Thus, for example, antiviral effects of the $cPLA_2\alpha$ inhibitor were not confirmed for HRV and PV (family *Picornaviridae*) (Fig. 9C, D). Also, vaccinia virus, a DNA

525 virus from the family *Poxviridae* that is known to induce major rearrangements of host cell
526 membranes, was not found to be affected by Py-2 (Fig. 9E). As another control, we included
527 IAV (family *Orthomyxoviridae)* in this study because this virus replicates in the nucleus and
528 does not produce membranous ROs in the host cell cytoplasm. Even with 40μM of Py-2, IAV
529 replication was not inhibited (Fig. 9F). Taken together, these data suggest critical (but
530 different) functions of cPLA$_2\alpha$ activity in the replication of viruses representing diferent virus
531 families.
532

Discussion

Despite their enormous genetic diversity, virtually all +RNA viruses employ specialized membrane compartments (ROs) as structural scaffolds for their multi-subunit replication machinery (60, 61). Because of their essential role in viral RNA synthesis, the viral and cellular factors involved in the formation of ROs are thought to represent potential drug targets for antiviral intervention and, in line with this, a number of small-molecule inhibitors of enzymes or signalling molecules involved in cellular lipid metabolism and membrane rearrangements have been reported to be effective against specific +RNA viruses or even a group of related viruses from the same genus or family (reviewed in (62)). However, there is also evidence that cellular factors and structures involved in the formation and function(s) of viral ROs are more diverse than previously thought, with significant differences being reported even for closely related viruses (63). The available evidence suggests that a detailed understanding of the RO structures of specific +RNA viruses and virus families will be required to identify suitable targets for therapeutic intervention. Obviously, the identification of essential factors and metabolic and/or signalling pathways conserved across different genera and families would be highly desirable, possibly paving the way for the development of broad-spectrum antivirals.

In this study, we have been able to show that the pharmacological inhibition of a cellular phospholipase, cPLA$_2\alpha$, using a specific small-molecule inhibitor drastically reduces coronavirus RNA synthesis and, as a consequence, protein accumulation and the production of infectious virus progeny. The data suggest that the inhibition of cPLA$_2\alpha$ activity blocks an early step in the viral replication cycle, most likely, the formation of virus-induced ROs. The cPLA$_2\alpha$ activity was confirmed to be required for coronavirus replication, as shown for HCoV-229E (genus *Alphacoronavirus*) and MERS-CoV (genus *Betacoronavirus*), but the cPLA$_2\alpha$ inhibitor was also effective against SFV, a member of the family *Togaviridae*, demonstrating that this phospholipase activity produces specific lipid compounds that are essential for the replication of phylogenetically diverse +RNA viruses. The precise role of

561 cPLA$_2\alpha$ in the production of fully functional ROs remains to be established. One of the
562 products generated by cPLA$_2\alpha$ is AA, an important signaling molecule and precursor of the
563 eicosanoid family of potent inflammatory mediators, such as prostaglandins, leukotrienes,
564 lipoxins, and thromboxanes (64). Among other functions, AA might indirectly affect
565 membrane formation and trafficking events by modulating specific signaling pathways in
566 coronavirus-infected cells. To address this possibility, we performed a small number of
567 experiments using inhibitors of COX1/2 and LOX, two key enzymes requiring AA as a
568 precursor. None of these inhibitors was found to have an effect on coronavirus replication
569 (Fig. 2A and (57)), contradicting a major role of AA-dependent pathways involving COX1/2
570 and LOX and their products in coronavirus replication, at least *in vitro*. Consistent with this
571 hypothesis, the addition of AA to the cell culture medium failed to restore coronavirus
572 replication in Py-2-treated cells (unpublished data). Based on this data and although we
573 cannot formally exclude other roles of AA in coronavirus replication, we consider it more
574 likely that the LPLs (rather than AA) produced by cPLA$_2\alpha$ have critical functions in
575 coronavirus replication and, particularly, in the formation of virus-induced ROs. LPLs are
576 found in relatively small amounts in biological membranes, yet play important roles in a wide
577 range of processes involving membrane remodeling as well as membrane/protein and
578 membrane/membrane interactions (65). Also, it is known that changes in the lipid
579 composition of membranes may be associated with membrane fusion and fission processes
580 (66). According to the “bilayer couple hypothesis” (67), the two leaflets of a lipid bilayer are
581 tightly coupled, with asymmetric changes in one leaflet having the potential to induce major
582 structural changes, such as membrane bending, fission and fusion (68-70). Thus, for
583 example, asymmetric cleavage of phospholipids in a lipid bilayer by cPLA$_2\alpha$ (the latter
584 converting cylindrical phospholipids into cone-shaped LPLs) can be expected to induce
585 membrane curvature which, in turn, may trigger the formation of vesicular membrane
586 structures as demonstrated previously for cPLA$_2\alpha$-mediated membrane-modulating activities
587 involved in tubulation and vesiculation processes of the Golgi complex, the vesiculation of
588 CD59-containing endosomes, and lipid droplet formation (71-74).

589

590 There is also evidence that, independent from its enzymatic activity, cPLA$_2\alpha$ may change the
591 membrane phospholipid packing through its hydrophobic C2 domain to induce the
592 membrane bending required for phagosome formation in macrophages (75, 76). In addition
593 to cPLA$_2\alpha$ and related phospholipases, a large number of other factors have been shown to
594 induce membrane curvature in diverse biological systems (for recent reviews, see (77-79)).
595
596 To provide additional evidence for specific lipid classes, particularly LPLs, playing an
597 important role in coronavirus replication, whole cell lipidome analyses of coronavirus-infected
598 cells were performed in this study. We were able to show that phoshatidic acid (PA) species
599 are downregulated whereas Cer and LPL species are upregulated in HCoV-229E-infected
600 cells (Fig. 8, Suppl. Table 1). PA is a key intermediate in the synthesis of
601 glycerophospholipids and triacylglycerids and an important lipid mediator that is involved in
602 diverse cellular functions including vesicular trafficking, cytoskeletal changes, secretion and
603 membrane alterations (80, 81). Possible biological implications of the observed
604 downregulation of PA remain to be studied.
605
606 The observed upregulation of bioactive Cer may indicate a cellular response to coronavirus
607 replication or even a possible role of Cer in supporting coronaviral replication. Cer is known
608 to induce apoptosis and autophagy (reviewed in (82)). It remains to be studied if (and to what
609 extent) Cer contributes to autophagy and apoptosis in coronavirus-infected cells. Both
610 processes have been suggested to be involved in coronavirus replication and represent
611 emerging fields of coronavirus research with partially controversial information being reported
612 for different viral and cellular systems (27, 28, 83-90).
613
614 Cer-rich domains are also known to increase the rigidity and stability of membranes. Cer is a
615 cone-shaped lipid that is able to induce negative curvature, thereby promoting inward
616 budding of membranes (91) and thus, possibly, facilitating the formation of DMVs. In support

617 of this, Cer was reported to be redistributed to West nile virus (WNV)-induced ROs in
618 infected Vero cells (92) while DENV, another member of the family of *Flaviviridae*, was found
619 to induce an increase in both Cer and LPL abundances in infected C6/36 mosquito cells (33).
620 Interestingly, the study by Atepe *et al.* (92) also showed that inhibition of Cer synthesis has
621 detrimental effects on WNV (strain Kunjin) replication while the replication of DENV serotype
622 2 strain New Guinea C was found to be enhanced, suggesting that the effects of Cer and
623 Cer-derived lipids on +RNA virus replication are complex and, potentially, virus (strain)
624 specific. Clearly, more studies are needed to obtain a better understanding of possible roles
625 of Cer in viral replication.
626
627 In the context of this study, it was of particular interest to show that there is a significant
628 increase of the LPL content in coronavirus-infected cells. This increase was not detected in
629 infected cells treated with cPLA$_2\alpha$ inhibitor, thus strongly supporting a critical involvement of
630 cPLA$_2\alpha$ activity in producing these increased LPL levels in infected cells. Furthermore, a co-
631 localization of dsRNA with *sn*-2-cleaved fluorogenic LPLs was observed by fluorescence
632 microscopy in virus-infected cells at 12 h p.i.. Together, these observations support the idea
633 that LPLs generated by cPLA$_2\alpha$ are functionally relevant components of ROs produced in
634 coronavirus-infected cells.
635
636 In a previous study, inhibition of cPLA$_2\alpha$ activity by Py-2 was shown to affect HCV replication
637 *in vitro* (40). However, in this case, the formation of HCV-induced ROs ('membranous web')
638 and viral RNA synthesis was not evidently affected. Instead, the production of infectious virus
639 progeny was found to be reduced, most probably, by a reduction of lipid droplets required for
640 HCV particle formation (40, 73). Furthermore, changes in the cellular lipidomes, including
641 LPLs, were reported for cells infected with HCV and DENV, respectively (33, 93), further
642 corroborating the hypothesis that LPLs have important but diverse functions in different
643 +RNA virus systems.
644

645 To explore potential inhibitory effects of Py-2, several other viruses known to rearrange
646 cellular membranes were included in this study. As mentioned above, the replication of
647 MERS-CoV (genus *Betacoronavirus*) and SFV (family *Togaviridae*) was inhibited in the
648 presence of Py-2, identifying cPLA$_2\alpha$ as an important host factor for +RNA virus replication.
649 By contrast, poliovirus 1 and human rhinovirus A1 (family *Picornaviridae*) were not affected
650 by the cPLA$_2\alpha$ inhibitor. Likewise, vaccinia virus (family *Poxviridae*), a DNA virus that is
651 known to induce major rearrangements of cytoplasmic membranes (25), was not inhibited by
652 the cPLA$_2\alpha$ inhibitor. Finally, influenza A virus, a negative-strand RNA virus that replicates in
653 the nucleus and does not induce specific ROs in the cytoplasm, was not affected by the
654 cPLA$_2\alpha$ inhibitor. Taken together, these inhibition data lead us to suggest that the formation
655 of ROs of coronaviruses and, possibly, several other +RNA viruses depend on specific LPLs
656 produced by cellular cPLA$_2\alpha$ activities. The selective inhibitory effects observed for members
657 of only a few +RNA virus families suggest very specific lipid requirements for these viruses
658 and contradict potential nonspecific/toxic effects being responsible for the observed antiviral
659 effects of Py-2 against corona- and alphaviruses. To our knowledge, the study provides the
660 first in-depth analysis of cellular lipidome changes in coronavirus-infected cells and adds to
661 the list of lipids and lipid-metabolizing enzymes confirmed to be involved in +RNA virus
662 replication and, possibly, suitable as targets for antiviral small-molecule inhibitors. However,
663 given the diverse structures, origins and lipid/protein compositions of virus-induced ROs, the
664 study supports previous conclusions that the inhibition of viral RO formation by targeting
665 highly (or even universally) conserved cellular factors remains a challenging goal (60, 61).
666

667 **Acknowledgments**

668 We would like to thank Christian Drosten (Berlin, Germany) for providing MERS-CoV
669 EMC/2012 and Nadja Karl, Anna Möbus, Sabine Agel und Barbara Hönig for excellent
670 technical assistance. The work was supported by the German Center for Infection Research
671 (DZIF), partner site Giessen, Germany (TTU Emerging Infections, to S.P. and J.Z.), and the
672 Deutsche Forschungsgemeinschaft (SFB 1021 'RNA viruses: RNA metabolism, host

673 response and pathogenesis'; projects A01 and C01, to J.Z. and S.P., respectively). The
674 funders had no role in study design, data collection and analysis, decision to publish, or
675 preparation of the manuscript. The authors declare no conflict of interest relating to this
676 study.

677

678 **Figure legends**

679

680 **Fig. 1. Production of infectious HCoV-229E progeny in cell culture is inhibited by the**
681 **cPLA$_2\alpha$ inhibitor Py-2. (A)** MTT assay of Huh-7, BEAS-B2 and MRC-5 cells, respectively,
682 that were treated with the indicated concentrations of Py-2 for 12 h. Cell viability was
683 determined using a tetrazolium-based reagent. **(B-D)** Virus titers (pfu/ml) in cell culture
684 supernatants collected from Py-2-treated and HCoV-229E-infected Huh-7 **(B)**, MRC-5 **(C)**,
685 and BEAS-B2 **(D)** cells, respectively, at 12 h p.i.. Cells were infected with an MOI of 3. At 2 h
686 p.i., the virus inocula were replaced with cell culture medium containing the indicated
687 concentrations of Py-2. **(E)** Growth curves of HCoV-229E in the presence or absence of Py-2
688 using Huh-7 cells infected at an MOI of 3. At 2 h p.i., the virus inocula were replaced with cell
689 culture medium containing the indicated concentrations of Py-2. Supernatants were collected
690 at 10, 12, 15, 21, and 24 h p.i., respectively, and virus titers were determined by plaque
691 assay.

692

693 **Fig. 2. Antiviral activities of the PLA$_2$ inhibitor AACOCF3 and of p38 and MEK**
694 **inhibitors in coronavirus replication. (A)** MTT assay of Huh-7 cells treated for 12 h with
695 the indicated concentrations of AACOCF3. Cell viability (compared to untreated cells) was
696 determined using a tetrazolium-based reagent. **(B)** Huh-7 cells were infected with HCoV-
697 229E (MOI of 3). After 2 h, the virus inoculum was replaced with cell culture medium
698 containing the indicated concentrations of AACOCF3. At 12 h p.i., cell culture supernatants
699 were collected and used to determine virus titers by focus-forming assay. **(C, D)** Huh-7 cells
700 were infected with HCoV-229E (MOI of 1) and treated with the indicated concentrations of
701 the p38 inhibitor SB203580 and/or the MEK inhibitor U0126 as indicated **(C)** or the
702 lipoxygenase inhibitor TEDC-2 **(D).** Virus titers in cell culture supernatants collected at 24 h
703 p.i. were determined by plaque assay. Significance levels were determined by two-tailed
704 unpaired Student's *t* test and are indicated in panels B and C as follows: * $p<0.05$; **
705 $p<0.005$; *** $p<0.0005$ (compared to untreated cells).

706

707 **Fig. 3. Time- and concentration-dependent inhibition of HCoV-229E replication in Huh-**
708 **7 cells by the cPLA$_2\alpha$ inhibitor Py-2. (A)** Immunofluorescence analysis of N protein
709 expression in Huh-7 cells infected with HCoV-229E at an MOI of 3 in the presence or
710 absence of 20 µM Py-2. **(B)** Western blot analysis of HCoV-229E nonstructural (nsp8) and
711 structural (N) protein accumulation at 12 h p.i. in Py-2-treated Huh-7 cells (MOI of 3). Actin
712 was used as loading control. **(C)** Northern blot analysis of viral RNA in HCoV-229E-infected
713 Huh-7 cells (MOI of 3) at 12 h p.i. Cells were kept in medium containing the indicated
714 concentrations of Py-2. The positions of viral genomic and major subgenomic RNAs (2, 4, 5,
715 6, and 7) are indicated. **(D)** Time-dependent antiviral effects of Py-2. HCoV-229E-infected
716 cells were treated with cPLA$_2\alpha$ inhibitor (20 µM Py-2) for different time periods p.i. as
717 indicated below. Production of infectious virus progeny was determined using (pooled) cell
718 culture supernatants collected until 12 h p.i.. Virus titers were determined and compared to
719 the titer determined for infected (but untreated) cells. Experiments were done in triplicate.
720 Significance levels determined by two-tailed unpaired Student's *t* test are indicated as
721 follows: * $p<0.05$; ** $p<0.005$; *** $p<0.0005$.

722

723 **Fig. 4. Inhibition of coronavirus RTC formation in Py-2-treated cells.** Huh-7 cells were
724 mock infected or infected with HCoV-229E (MOI of 3) and incubated in the presence or
725 absence of 20 µM Py-2 as indicated. At 12 h p.i., the cells were fixed with 3.7%
726 paraformaldehyde and analyzed by immunofluorescence microscopy using antibodies
727 specific for dsRNA (red signal) and nonstructural protein 8 (nsp8; green signal), respectively,
728 to monitor the formation of viral RTCs in infected cells.

729

730 **Fig. 5. Immunofluorescence analysis of dsRNA and nascent RNA in HCoV-229E-**
731 **infected cells. (A)** 3D immunofluorescence analysis of Z-stacks (Imaris) of representative
732 HCoV-229E-infected Huh-7 cells (MOI of 3) in the absence or presence of 20 µM Py-2 using
733 a dsRNA-specific antibody (red signal). **(B)** Huh-7 cells were infected with HCoV-229E (MOI

734 of 3). At 1 h p.i., the virus inoclum was replaced with medium containing 20 µM actinomycin
735 D to inhibit cellular DNA-dependent RNA synthesis. At 11 h p.i., the cell culture medium was
736 supplemented with 1 mM 5-EU. At 12 h p.i., the cells were fixed and detection of
737 incorporated alkyne-modified 5-EU was detected using click chemistry (see Material and
738 Methods). Nuclei were stained with DAPI (blue signal) and dsRNA was stained using a
739 dsRNA-specific mAb (red signal).
740
741 **Fig. 6. Py-2 reduces the formation of DMVs.** Huh-7 cells were infected with HCoV-229E
742 (MOI of 3) and incubated in the absence **(A, B)** or presence **(C, D)** of 20 µM Py-2 in the cell
743 culture medium. At 12 h p.i., the cells were fixed with glutaraldehyde, embedded and
744 analyzed by transmission electron microscopy (EM912a/b; Zeiss) at 120 kV. The
745 representative images included in this figure were selected from >100 images captured in
746 two independent experiments (see below). **(E, F)** Time-dependent effects of Py-2 on DMV
747 and intracellular virus (ICV) production in HCoV-229E-infected cells. Py-2 (20 µM) was
748 included in the cell culture medium for the indicated times p.i.. Inf, HCoV-infected cells
749 without inhibitor. **(E)** Percentage of cells in which DMVs and ICVs, respectively, could be
750 identified (for details, see Material and Methods). **(F)** Numbers of DMVs detected per cell (for
751 details, see Material and Methods). Significance levels determined by two-tailed unpaired
752 Student's *t* test are indicated in panels **E** and **F** as follows: * $p<0.05$; ** $p<0.005$; *** $p<0.0005$
753 (compared to untreated cells; n(inf) = 154, n(2-12 h) = 190, n(2-7h) = 135, n(7-12h) = 107)
754
755 **Fig. 7. Coronavirus RTCs colocalize with LPLs produced by cPLA$_2\alpha$ activity.** Huh-7
756 cells were infected with HCoV-229E (MOI of 3) and incubated with PC-A2, a fluorogenic
757 PLA$_2\alpha$ substrate suitable to detect LPLs produced by cPLA$_2\alpha$ cleavage at the *sn*-2 position of
758 phospholipids. At 12 h p.i., the cells were fixed and immunostained for dsRNA. Colocalization
759 signals were calculated for the total images shown in rows 3, 4 and 5, 6, respectively, and
760 are displayed separately (right column). Colocalization rates and PCCs are indicated (for

details, see Material and Methods). Insets indicate regions of interest displayed at higher magnification in the next row.

Fig. 8. Coronavirus replication is associated with an increase of the cellular LPL content. Quantities of selected lipid classes and categories were determined using shotgun lipidomics. Shown are the results for Huh-7 cells alone, Huh-7 cells incubated with UV-inactivated HCoV-229E, Huh-7 cells infected with HCoV-229E, and Huh-7 cells infected with HCoV-229E and treated with 20 μM Py-2 as indicated to the left. **(A)** Abundance of all membrane lipids detected in the samples. **(B)** Abundance of neutral lipids representing the sum of triacylglycerols (TAG), diacylglycerol (DAG), and cholesterylesters (CE). Also shown are the abundances of phosphatidic acids (PA) **(C)**, ceramides **(D)**, lysophospholipids (LPL) **(E)** and phosphatidylglycerols (PG) **(F)**. Significance levels were determined by two-tailed unpaired Student's *t* test and are indicated as follows: * $p<0.05$; ** $p<0.005$; *** $p<0.0005$. For a complete data set of individual lipid species, see Supplemental Tables 1 and 2. Abundances are given in arbitrary units (a.u.).

Fig. 9. Effects of cPLA$_2\alpha$ inhibition on the replication of other viruses. Cells were infected with MERS-CoV (Huh-7, Vero) **(A)**, SFV (BHK-21) **(B)**, human rhinovirus 1A (HeLa) **(C)**, poliovirus (Vero) **(D)**, vaccinia virus (Huh-7) **(E)**, and influenza A virus (A549) **(F)**, respectively, with an MOI of 3. At 2 h p.i., the virus inocula were replaced with medium supplemented with the indicated concentrations of Py-2. At 12 h p.i., supernatants were collected and virus titers were determined by focus-forming assay (ffu/ml) or plaque assay (pfu/ml). Experiments were done in triplicate. Significance levels were determined by two-tailed unpaired Student's *t* test and are indicated as follows: * $p<0.05$; ** $p<0.005$ (compared to titers obtained with untreated cells).

789

790

791

792 **References**

793

794 1. de Groot RJ, Baker SC, Baric R, Enjuanes L, Gorbalenya AE, Holmes KV, Perlman S,
795 Poon L, Rottier PJM, Talbot PJ, Woo PCY, Ziebuhr J. 2012. Family *Coronaviridae*, p
796 806-828. *In* King AMQ, Adams MJ, Carstens EB, Lefkowitz EJ (ed), Virus Taxonomy.
797 Elsevier, Amsterdam.
798 2. de Groot RJ, Cowley JA, Enjuanes L, Faaberg KS, Perlman S, Rottier PJM, Snijder EJ,
799 Ziebuhr J, Gorbalenya AE. 2012. Order *Nidovirales*, p 785-795. *In* King AMQ, Adams
800 MJ, Carstens EB, Lefkowitz EJ (ed), Virus Taxonomy. Elsevier, Amsterdam.
801 3. van der Hoek L. 2007. Human coronaviruses: what do they cause? Antiviral therapy
802 12:651-658.
803 4. Drosten C, Gunther S, Preiser W, van der Werf S, Brodt HR, Becker S, Rabenau H,
804 Panning M, Kolesnikova L, Fouchier RA, Berger A, Burguiere AM, Cinatl J, Eickmann M,
805 Escriou N, Grywna K, Kramme S, Manuguerra JC, Muller S, Rickerts V, Sturmer M,
806 Vieth S, Klenk HD, Osterhaus AD, Schmitz H, Doerr HW. 2003. Identification of a novel
807 coronavirus in patients with severe acute respiratory syndrome. N Engl J Med 348:1967-
808 1976.
809 5. Peiris JS, Yuen KY, Osterhaus AD, Stohr K. 2003. The severe acute respiratory
810 syndrome. The New England journal of medicine 349:2431-2441.
811 6. Zaki AM, van Boheemen S, Bestebroer TM, Osterhaus ADME, Fouchier RAM. 2012.
812 Isolation of a novel coronavirus from a man with pneumonia in Saudi Arabia. N Engl J
813 Med 367:1814-1820.
814 7. Peiris JS, Lai ST, Poon LL, Guan Y, Yam LY, Lim W, Nicholls J, Yee WK, Yan WW,
815 Cheung MT, Cheng VC, Chan KH, Tsang DN, Yung RW, Ng TK, Yuen KY. 2003.
816 Coronavirus as a possible cause of severe acute respiratory syndrome. Lancet
817 361:1319-1325.
818 8. Zumla A, Hui DS, Perlman S. 2015. Middle East respiratory syndrome. Lancet 386:995-
819 1007.

9. Angelini MM, Neuman BW, Buchmeier MJ. 2014. Untangling membrane rearrangement in the nidovirales. DNA Cell Biol 33:122-127.
10. V'Kovski P, Al-Mulla H, Thiel V, Neuman BW. 2015. New insights on the role of paired membrane structures in coronavirus replication. Virus Res 202:33-40.
11. Ahlquist P. 2006. Parallels among positive-strand RNA viruses, reverse-transcribing viruses and double-stranded RNA viruses. Nature Reviews Microbiology 4:371-382.
12. den Boon JA, Ahlquist P. 2010. Organelle-like membrane compartmentalization of positive-strand RNA virus replication factories. Annu Rev Microbiol 64:241-256.
13. den Boon JA, Diaz A, Ahlquist P. 2010. Cytoplasmic viral replication complexes. Cell Host Microbe 8:77-85.
14. Angelini MM, Akhlaghpour M, Neuman BW, Buchmeier MJ. 2013. Severe acute respiratory syndrome coronavirus nonstructural proteins 3, 4, and 6 induce double-membrane vesicles. MBio 4.
15. Baliji S, Cammer SA, Sobral B, Baker SC. 2009. Detection of nonstructural protein 6 in murine coronavirus-infected cells and analysis of the transmembrane topology by using bioinformatics and molecular approaches. J Virol 83:6957-6962.
16. Oostra M, Hagemeijer MC, van Gent M, Bekker CP, te Lintelo EG, Rottier PJ, de Haan CA. 2008. Topology and membrane anchoring of the coronavirus replication complex: not all hydrophobic domains of nsp3 and nsp6 are membrane spanning. J Virol 82:12392-12405.
17. Perlman S, Netland J. 2009. Coronaviruses post-SARS: update on replication and pathogenesis. Nat Rev Microbiol 7:439-450.
18. Ulasli M, Verheije MH, de Haan CAM, Reggiori F. 2010. Qualitative and quantitative ultrastructural analysis of the membrane rearrangements induced by coronavirus. Cell Microbiol 12:844-861.
19. Hagemeijer MC, Verheije MH, Ulasli M, Shaltiël IA, de Vries LA, Reggiori F, Rottier PJM, de Haan CAM. 2010. Dynamics of coronavirus replication-transcription complexes. J Virol 84:2134-2149.

20. Hagemeijer MC, Vonk AM, Monastyrska I, Rottier PJM, de Haan CAM. 2012. Visualizing coronavirus RNA synthesis in time by using click chemistry. J Virol 86:5808-5816.
21. Knoops K, Bárcena M, Limpens RWAL, Koster AJ, Mommaas AM, Snijder EJ. 2012. Ultrastructural characterization of arterivirus replication structures: reshaping the endoplasmic reticulum to accommodate viral RNA synthesis. J Virol 86:2474-2487.
22. Snijder EJ, van der Meer Y, Zevenhoven-Dobbe J, Onderwater JJM, van der Meulen J, Koerten HK, Mommaas AM. 2006. Ultrastructure and origin of membrane vesicles associated with the severe acute respiratory syndrome coronavirus replication complex. J Virol 80:5927-5940.
23. Gosert R, Kanjanahaluethai A, Egger D, Bienz K, Baker SC. 2002. RNA replication of mouse hepatitis virus takes place at double-membrane vesicles. J Virol 76:3697-3708.
24. Knoops K, Kikkert M, Worm SH, Zevenhoven-Dobbe JC, van der Meer Y, Koster AJ, Mommaas AM, Snijder EJ. 2008. SARS-coronavirus replication is supported by a reticulovesicular network of modified endoplasmic reticulum. PLoS Biol 6:e226.
25. Sodeik B, Krijnse-Locker J. 2002. Assembly of vaccinia virus revisited: de novo membrane synthesis or acquisition from the host? Trends Microbiol 10:15-24.
26. Knoops K, Swett-Tapia C, van den Worm SH, Te Velthuis AJ, Koster AJ, Mommaas AM, Snijder EJ, Kikkert M. 2010. Integrity of the early secretory pathway promotes, but is not required for, severe acute respiratory syndrome coronavirus RNA synthesis and virus-induced remodeling of endoplasmic reticulum membranes. J Virol 84:833-846.
27. Reggiori F, Monastyrska I, Verheije MH, Cali T, Ulasli M, Bianchi S, Bernasconi R, de Haan CA, Molinari M. 2010. Coronaviruses Hijack the LC3-I-positive EDEMosomes, ER-derived vesicles exporting short-lived ERAD regulators, for replication. Cell Host Microbe 7:500-508.
28. Maier HJ, Britton P. 2012. Involvement of autophagy in coronavirus replication. Viruses 4:3440-3451.
29. Reid CR, Airo AM, Hobman TC. 2015. The Virus-Host Interplay: Biogenesis of +RNA Replication Complexes. Viruses 7:4385-4413.

30. Heaton NS, Perera R, Berger KL, Khadka S, Lacount DJ, Kuhn RJ, Randall G. 2010. Dengue virus nonstructural protein 3 redistributes fatty acid synthase to sites of viral replication and increases cellular fatty acid synthesis. Proc Natl Acad Sci U S A 107:17345-17350.
31. Greseth MD, Traktman P. 2014. De novo fatty acid biosynthesis contributes significantly to establishment of a bioenergetically favorable environment for vaccinia virus infection. PLoS Pathog 10:e1004021.
32. Martin-Acebes MA, Blazquez AB, Jimenez de Oya N, Escribano-Romero E, Saiz JC. 2011. West Nile virus replication requires fatty acid synthesis but is independent on phosphatidylinositol-4-phosphate lipids. PLoS One 6:e24970.
33. Perera R, Riley C, Isaac G, Hopf-Jannasch AS, Moore RJ, Weitz KW, Pasa-Tolic L, Metz TO, Adamec J, Kuhn RJ. 2012. Dengue virus infection perturbs lipid homeostasis in infected mosquito cells. PLoS Pathog 8:e1002584.
34. Sagan SM, Rouleau Y, Leggiadro C, Supekova L, Schultz PG, Su AI, Pezacki JP. 2006. The influence of cholesterol and lipid metabolism on host cell structure and hepatitis C virus replication. Biochem Cell Biol 84:67-79.
35. Yang W, Hood BL, Chadwick SL, Liu S, Watkins SC, Luo G, Conrads TP, Wang T. 2008. Fatty acid synthase is up-regulated during hepatitis C virus infection and regulates hepatitis C virus entry and production. Hepatology 48:1396-1403.
36. Balsinde J, Winstead MV, Dennis EA. 2002. Phospholipase A(2) regulation of arachidonic acid mobilization. FEBS Lett 531:2-6.
37. Murakami M, Taketomi Y, Miki Y, Sato H, Hirabayashi T, Yamamoto K. 2011. Recent progress in phospholipase A(2) research: from cells to animals to humans. Prog Lipid Res 50:152-192.
38. Ghosh M, Tucker DE, Burchett SA, Leslie CC. 2006. Properties of the Group IV phospholipase A2 family. Prog Lipid Res 45:487-510.
39. Lin LL, Wartmann M, Lin AY, Knopf JL, Seth A, Davis RJ. 1993. cPLA2 is phosphorylated and activated by MAP kinase. Cell 72:269-278.

40. Menzel N, Fischl W, Hueging K, Bankwitz D, Frentzen A, Haid S, Gentzsch J, Kaderali L, Bartenschlager R, Pietschmann T. 2012. MAP-kinase regulated cytosolic phospholipase A2 activity is essential for production of infectious hepatitis C virus particles. PLoS Pathog 8:e1002829.
41. Seno K, Okuno T, Nishi K, Murakami Y, Watanabe F, Matsuura T, Wada M, Fujii Y, Yamada M, Ogawa T, Okada T, Hashizume H, Kii M, Hara S, Hagishita S, Nakamoto S, Yamada K, Chikazawa Y, Ueno M, Teshirogi I, Ono T, Ohtani M. 2000. Pyrrolidine inhibitors of human cytosolic phospholipase A(2). J Med Chem 43:1041-1044.
42. Street IP, Lin HK, Laliberte F, Ghomashchi F, Wang Z, Perrier H, Tremblay NM, Huang Z, Weech PK, Gelb MH. 1993. Slow- and tight-binding inhibitors of the 85-kDa human phospholipase A2. Biochemistry 32:5935-5940.
43. Mosmann T. 1983. Rapid colorimetric assay for cellular growth and survival: application to proliferation and cytotoxicity assays. J Immunol Methods 65:55-63.
44. Ziebuhr J, Siddell SG. 1999. Processing of the human coronavirus 229E replicase polyproteins by the virus-encoded 3C-like proteinase: identification of proteolytic products and cleavage sites common to pp1a and pp1ab. J Virol 73:177-185.
45. Thiel V, Ivanov KA, Putics A, Hertzig T, Schelle B, Bayer S, Weissbrich B, Snijder EJ, Rabenau H, Doerr HW, Gorbalenya AE, Ziebuhr J. 2003. Mechanisms and enzymes involved in SARS coronavirus genome expression. J Gen Virol 84:2305-2315.
46. Dunn KW, Kamocka MM, McDonald JH. 2011. A practical guide to evaluating colocalization in biological microscopy. Am J Physiol Cell Physiol 300:C723-742.
47. Manders EM, Stap J, Brakenhoff GJ, van Driel R, Aten JA. 1992. Dynamics of three-dimensional replication patterns during the S-phase, analysed by double labelling of DNA and confocal microscopy. J Cell Sci 103 (Pt 3):857-862.
48. Manders EM, Verbeek FJ, Aten JA. 1993. Measurement of co-localization of objects in dual-colour confocal images. J Microsc 169:375-382.

930 49. Adler J, Parmryd I. 2010. Quantifying colocalization by correlation: the Pearson
931 correlation coefficient is superior to the Mander's overlap coefficient. Cytometry 77A:733-
932 742.
933 50. Barlow AL, Macleod A, Noppen S, Sanderson J, Guerin CJ. 2010. Colocalization
934 analysis in fluorescence micrographs: verification of a more accurate calculation of
935 pearson's correlation coefficient. Microsc Microanal 16:710-724.
936 51. Costes SV, Daelemans D, Cho EH, Dobbin Z, Pavlakis G, Lockett S. 2004. Automatic
937 and quantitative measurement of protein-protein colocalization in live cells. Biophys J
938 86:3993-4003.
939 52. Matyash V, Liebisch G, Kurzchalia TV, Shevchenko A, Schwudke D. 2008. Lipid
940 extraction by methyl-tert-butyl ether for high-throughput lipidomics. J Lipid Res 49:1137-
941 1146.
942 53. Herzog R, Schuhmann K, Schwudke D, Sampaio JL, Bornstein SR, Schroeder M,
943 Shevchenko A. 2012. LipidXplorer: a software for consensual cross-platform lipidomics.
944 PLoS One 7:e29851.
945 54. Herzog R, Schwudke D, Shevchenko A. 2013. LipidXplorer: Software for Quantitative
946 Shotgun Lipidomics Compatible with Multiple Mass Spectrometry Platforms. Curr Protoc
947 Bioinformatics 43:14 12 11-30.
948 55. Schwudke D, Liebisch G, Herzog R, Schmitz G, Shevchenko A. 2007. Shotgun
949 lipidomics by tandem mass spectrometry under data-dependent acquisition control.
950 Methods Enzymol 433:175-191.
951 56. Schwudke D, Schuhmann K, Herzog R, Bornstein SR, Shevchenko A. 2011. Shotgun
952 lipidomics on high resolution mass spectrometers. Cold Spring Harb Perspect Biol
953 3:a004614.
954 57. Müller C, Karl N, Ziebuhr J, Pleschka S. 2016. D, L-lysine acetylsalicylate + glycine
955 impairs coronavirus replication. J Antivir Antiretrovir 8:142-150.

956 58. Heusipp G, Grotzinger C, Herold J, Siddell SG, Ziebuhr J. 1997. Identification and
957 subcellular localization of a 41 kDa, polyprotein 1ab processing product in human
958 coronavirus 229E-infected cells. J Gen Virol 78 (Pt 11):2789-2794.
959 59. Jao CY, Salic A. 2008. Exploring RNA transcription and turnover in vivo by using click
960 chemistry. Proc Natl Acad Sci U S A 105:15779-15784.
961 60. Romero-Brey I, Bartenschlager R. 2014. Membranous replication factories induced by
962 plus-strand RNA viruses. Viruses 6:2826-2857.
963 61. Strating JR, van Kuppeveld FJ. 2017. Viral rewiring of cellular lipid metabolism to create
964 membranous replication compartments. Curr Opin Cell Biol 47:24-33.
965 62. Konan KV, Sanchez-Felipe L. 2014. Lipids and RNA virus replication. Curr Opin Virol
966 9:45-52.
967 63. Dorobantu CM, Albulescu L, Harak C, Feng Q, van Kampen M, Strating JR, Gorbalenya
968 AE, Lohmann V, van der Schaar HM, van Kuppeveld FJ. 2015. Modulation of the Host
969 Lipid Landscape to Promote RNA Virus Replication: The Picornavirus
970 Encephalomyocarditis Virus Converges on the Pathway Used by Hepatitis C Virus.
971 PLoS Pathog 11:e1005185.
972 64. Harizi H, Corcuff JB, Gualde N. 2008. Arachidonic-acid-derived eicosanoids: roles in
973 biology and immunopathology. Trends Mol Med 14:461-469.
974 65. Mishima K, Nakajima M, Ogihara T. 2004. Effects of lysophospholipids on membrane
975 order of phosphatidylcholine. Colloids and Surfaces B-Biointerfaces 33:185-189.
976 66. Roux A, Cuvelier D, Nassoy P, Prost J, Bassereau P, Goud B. 2005. Role of curvature
977 and phase transition in lipid sorting and fission of membrane tubules. EMBO J 24:1537-
978 1545.
979 67. Sheetz MP, Singer SJ. 1974. Biological membranes as bilayer couples. A molecular
980 mechanism of drug-erythrocyte interactions. Proc Natl Acad Sci U S A 71:4457-4461.
981 68. Burger KN. 2000. Greasing membrane fusion and fission machineries. Traffic 1:605-613.
982 69. Huttner WB, Schmidt AA. 2002. Membrane curvature: a case of endofeelin'. Trends Cell
983 Biol 12:155-158.

70. Zimmerberg J, Gawrisch K. 2006. The physical chemistry of biological membranes. Nat Chem Biol 2:564-567.
71. Brown WJ, Chambers K, Doody A. 2003. Phospholipase A2 (PLA2) enzymes in membrane trafficking: mediators of membrane shape and function. Traffic 4:214-221.
72. de Figueiredo P, Drecktrah D, Katzenellenbogen JA, Strang M, Brown WJ. 1998. Evidence that phospholipase A2 activity is required for Golgi complex and trans Golgi network membrane tubulation. Proc Natl Acad Sci U S A 95:8642-8647.
73. Gubern A, Casas J, Barcelo-Torns M, Barneda D, de la Rosa X, Masgrau R, Picatoste F, Balsinde J, Balboa MA, Claro E. 2008. Group IVA phospholipase A2 is necessary for the biogenesis of lipid droplets. J Biol Chem 283:27369-27382.
74. Cai B, Caplan S, Naslavsky N. 2012. cPLA2alpha and EHD1 interact and regulate the vesiculation of cholesterol-rich, GPI-anchored, protein-containing endosomes. Mol Biol Cell 23:1874-1888.
75. Gallop JL, McMahon HT. 2005. BAR domains and membrane curvature: bringing your curves to the BAR. Biochem Soc Symp:223-231.
76. Zizza P, Iurisci C, Bonazzi M, Cossart P, Leslie CC, Corda D, Mariggio S. 2012. Phospholipase A2IValpha regulates phagocytosis independent of its enzymatic activity. J Biol Chem 287:16849-16859.
77. Brown MF. 2012. Curvature forces in membrane lipid-protein interactions. Biochemistry 51:9782-9795.
78. Jarsch IK, Daste F, Gallop JL. 2016. Membrane curvature in cell biology: An integration of molecular mechanisms. J Cell Biol 214:375-387.
79. McMahon HT, Boucrot E. 2015. Membrane curvature at a glance. J Cell Sci 128:1065-1070.
80. Wang X, Devaiah SP, Zhang W, Welti R. 2006. Signaling functions of phosphatidic acid. Prog Lipid Res 45:250-278.
81. Athenstaedt K, Daum G. 2006. The life cycle of neutral lipids: synthesis, storage and degradation. Cell Mol Life Sci 63:1355-1369.

1012 82. Gault CR, Obeid LM, Hannun YA. 2010. An overview of sphingolipid metabolism: from
1013 synthesis to breakdown. Adv Exp Med Biol 688:1-23.
1014 83. Fung TS, Liu DX. 2014. Coronavirus infection, ER stress, apoptosis and innate
1015 immunity. Front Microbiol 5:296.
1016 84. Cong Y, Verlhac P, Reggiori F. 2017. The Interaction between Nidovirales and
1017 Autophagy Components. Viruses 9:182.
1018 85. de Haan CA, Reggiori F. 2008. Are nidoviruses hijacking the autophagy machinery?
1019 Autophagy 4:276-279.
1020 86. Prentice E, Jerome WG, Yoshimori T, Mizushima N, Denison MR. 2004. Coronavirus
1021 replication complex formation utilizes components of cellular autophagy. J Biol Chem
1022 279:10136-10141.
1023 87. Snijder EJ, van der Meer Y, Zevenhoven-Dobbe J, Onderwater JJ, van der Meulen J,
1024 Koerten HK, Mommaas AM. 2006. Ultrastructure and origin of membrane vesicles
1025 associated with the severe acute respiratory syndrome coronavirus replication complex.
1026 J Virol 80:5927-5940.
1027 88. Zhao Z, Thackray LB, Miller BC, Lynn TM, Becker MM, Ward E, Mizushima NN, Denison
1028 MR, Virgin HWt. 2007. Coronavirus replication does not require the autophagy gene
1029 ATG5. Autophagy 3:581-585.
1030 89. Cottam EM, Maier HJ, Manifava M, Vaux LC, Chandra-Schoenfelder P, Gerner W,
1031 Britton P, Ktistakis NT, Wileman T. 2011. Coronavirus nsp6 proteins generate
1032 autophagosomes from the endoplasmic reticulum via an omegasome intermediate.
1033 Autophagy 7:1335-1347.
1034 90. Maier HJ, Cottam EM, Stevenson-Leggett P, Wilkinson JA, Harte CJ, Wileman T, Britton
1035 P. 2013. Visualizing the autophagy pathway in avian cells and its application to studying
1036 infectious bronchitis virus. Autophagy 9:496-509.
1037 91. Utermohlen O, Herz J, Schramm M, Kronke M. 2008. Fusogenicity of membranes: the
1038 impact of acid sphingomyelinase on innate immune responses. Immunobiology 213:307-
1039 314.

1040 92. Aktepe TE, Pham H, Mackenzie JM. 2015. Differential utilisation of ceramide during
1041 replication of the flaviviruses West Nile and dengue virus. Virology 484:241-250.
1042 93. Roe B, Kensicki E, Mohney R, Hall WW. 2011. Metabolomic profile of hepatitis C virus-
1043 infected hepatocytes. PLoS One 6:e23641.

1044

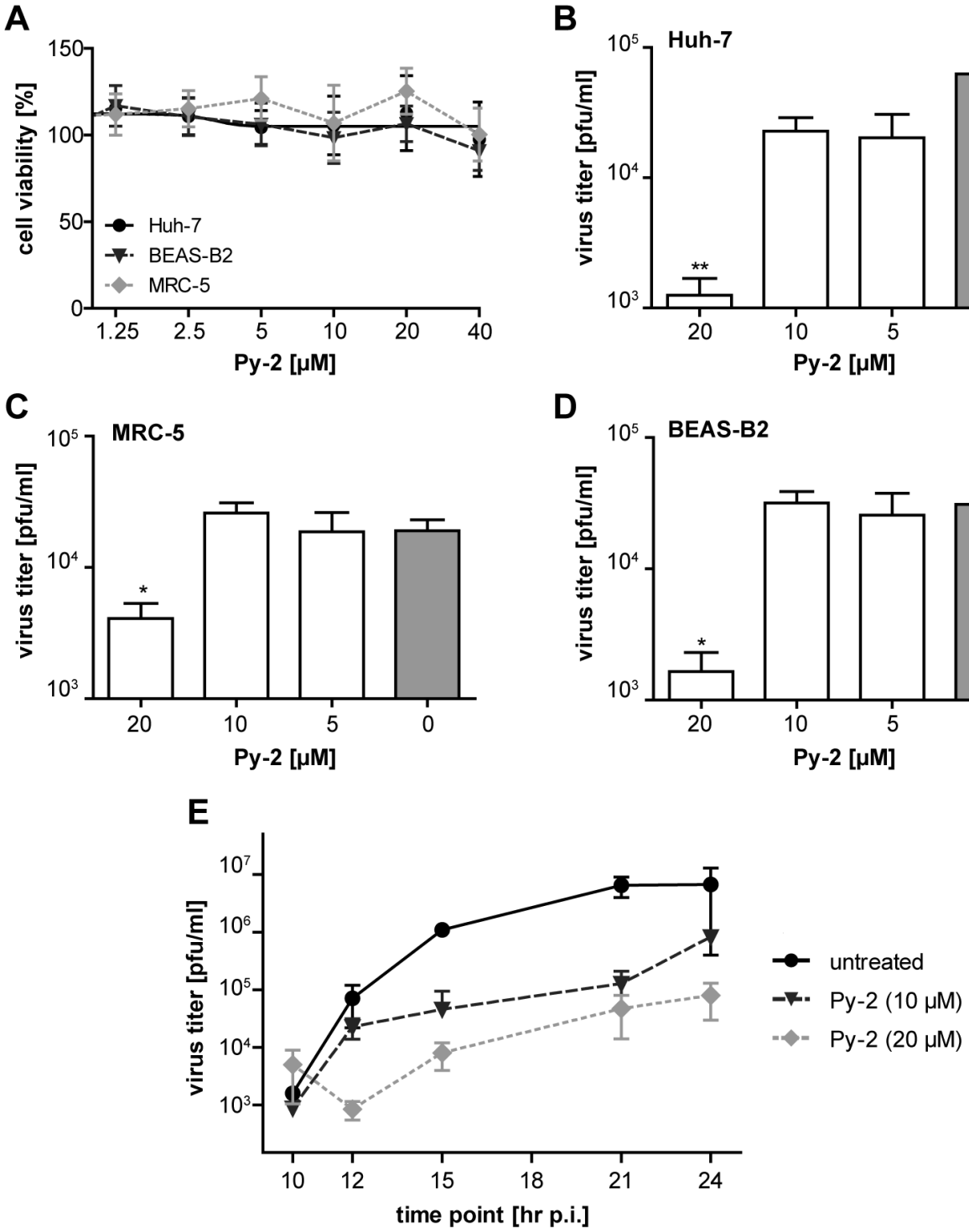

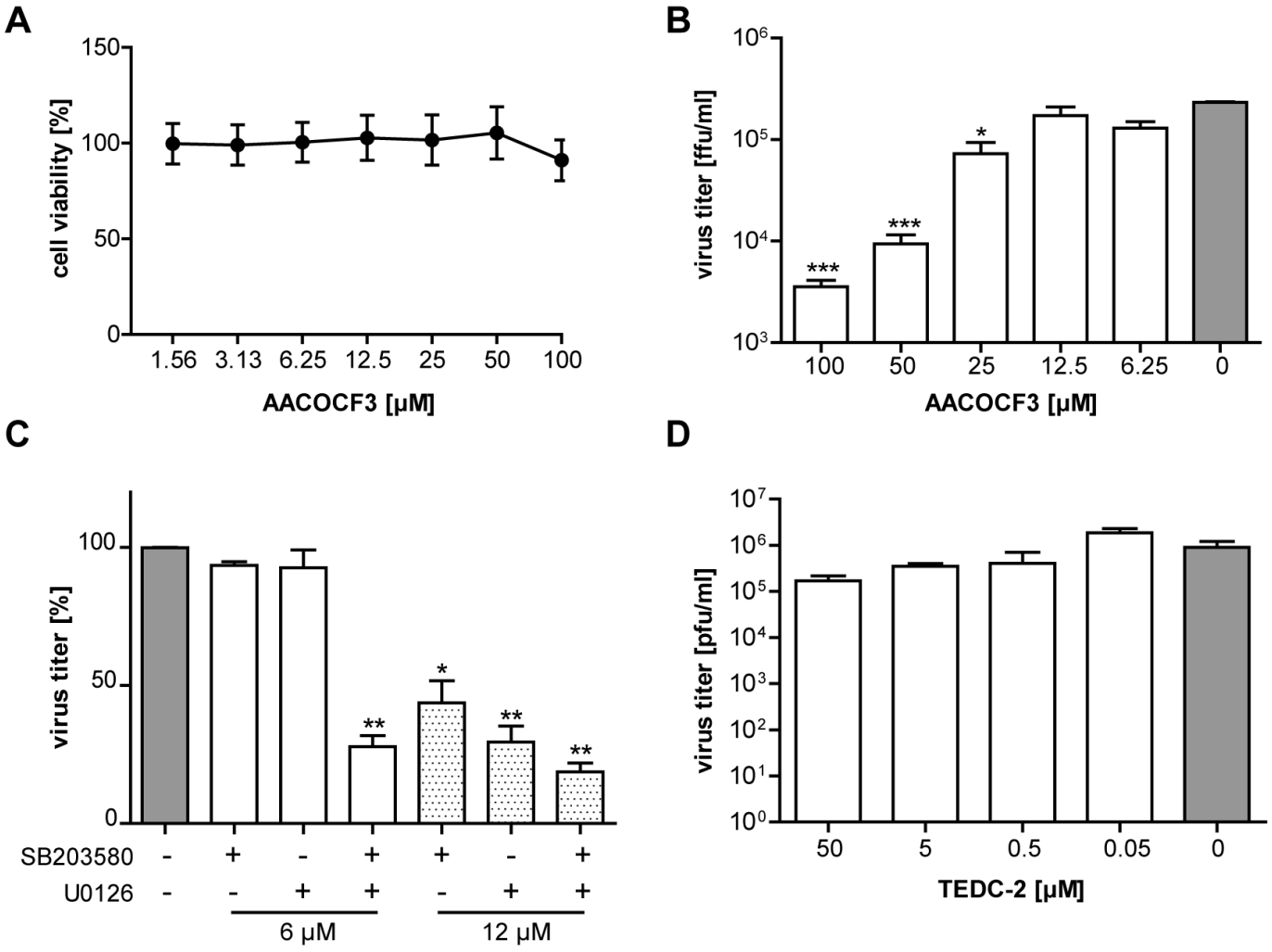

A

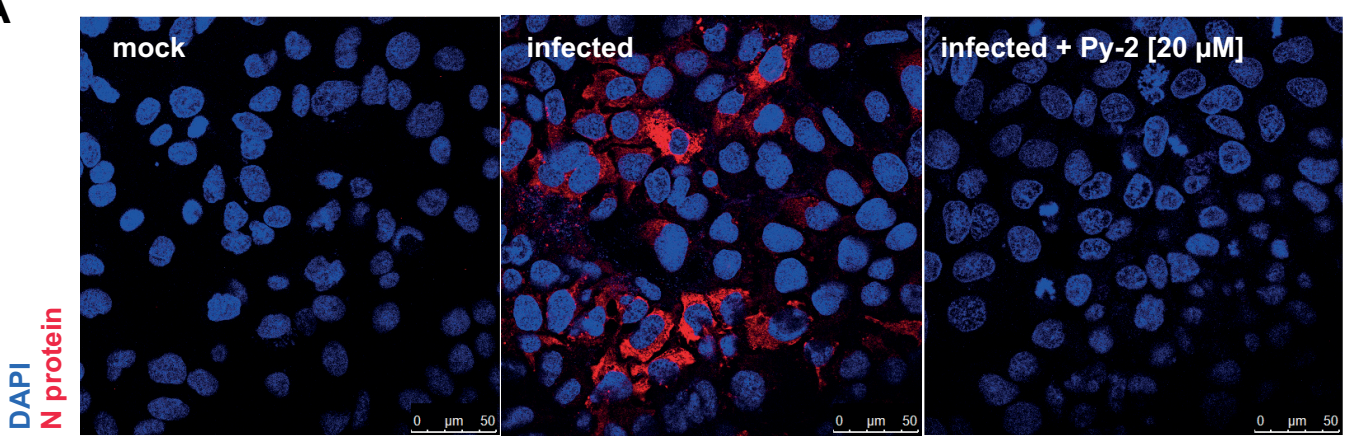

B

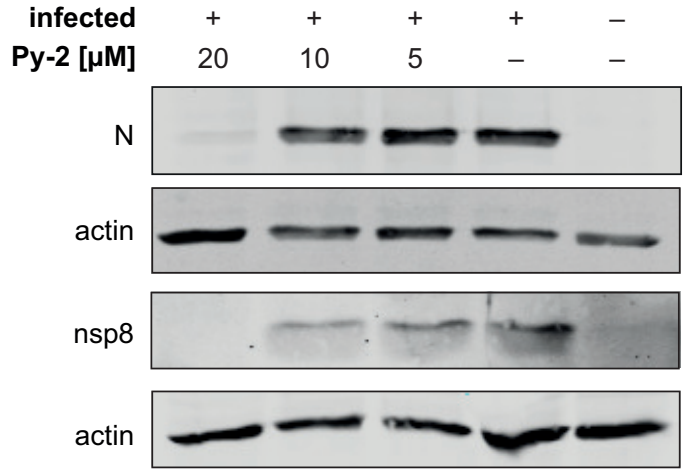

C

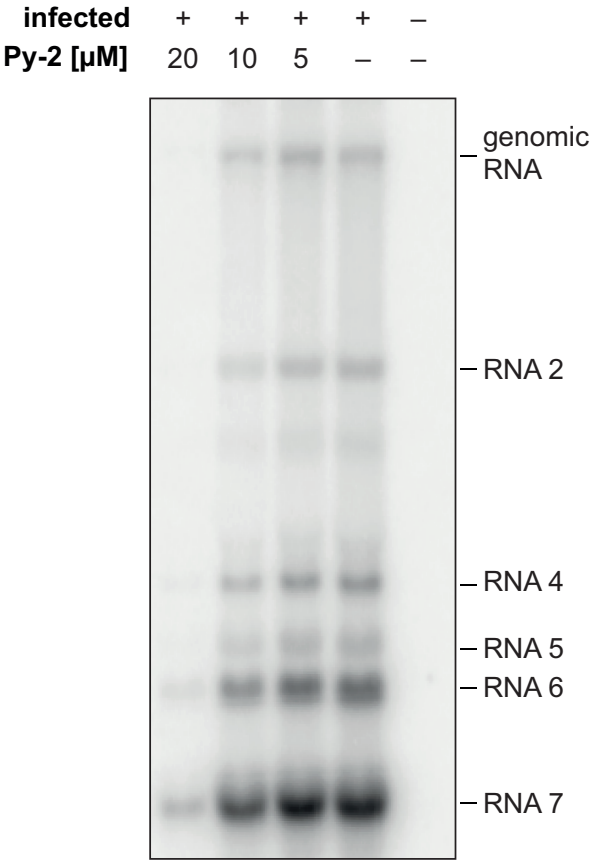

D